JOURNAL OF GEOPHYSICAL RESEARCH, VOL. 94, NO. D9, PAGES 11,625–11,640, AUGUST 30, 1989

Potential Vorticity and Mixing in the South Polar Vortex During Spring

D. L. HARTMANN,[1] K. R. CHAN,[2] B. L. GARY,[3] M. R. SCHOEBERL,[4]
P. A. NEWMAN,[4] R. L. MARTIN,[4] M. LOEWENSTEIN,[2]
J. R. PODOLSKE,[2] AND S. E. STRAHAN[2]

A central part of the explanation of the Antarctic ozone hole is the dynamical isolation provided by the intense vortex present over the south polar region until late in the spring. In this paper some fluid dynamical aspects of the Antarctic ozone hole phenomena are investigated, using data collected by the ER-2 aircraft during the Airborne Antarctic Ozone Experiment (AAOE). Analysis of high-resolution potential vorticity and nitrous oxide sections determined from the aircraft data show relatively little evidence of irreversible lateral mixing associated with large-scale disturbances. Less than 10% of the flight legs show evidence of reversed meridional gradients of potential vorticity and nitrous oxide for spatial scales of more than a few degrees of latitude. Correlation studies show that small-scale static stability variations are correlated positively with wind speed and not with relative vorticity, which strongly suggests that these are gravity wave signatures. Smaller-scale variations in nitrous oxide and wind velocity are thus believed to be associated with gravity waves and not to represent lateral mixing which would constitute a significant breach of the dynamical isolation implied by the large-scale potential vorticity gradient. Compositing of wind, potential vorticity, and nitrous oxide relative to the edge of the chemically perturbed region shows an enhancement of the meridional gradient of potential vorticity and nitrous oxide near this boundary at the 450 K potential temperature level. It is argued that this may be caused by the developing ozone concentration gradient producing a strong gradient in solar heating, which in turn drives a steepened potential vorticity gradient, although the temporal sampling provided by the AAOE measurements is not sufficient to prove this hypothesis. Another possible explanation of the enhanced gradients would be gradient steepening through erosion, by lateral mixing on the inner edge of the region of the strong meridional gradients of conserved quantities that define the vortex.

1. INTRODUCTION

A key component of the "Antarctic ozone hole" phenomenon is the dynamical isolation provided by the south polar vortex. Strong radiative forcing in fall and winter drives the southern stratosphere toward an equilibrium characterized by a cold, intense vortex. Relatively weak wave driving, resulting from weak zonal asymmetries in surface conditions, yields a balance in the lower stratosphere that is near radiative equilibrium compared to conditions in the northern hemisphere. This mean state is characterized by intense westerly winds in the stratosphere and by strong meridional gradients of potential vorticity and nitrous oxide on isentropic surfaces. Such gradients indicate that irreversible mixing of parcels of air across latitude belts is weak and that the core of the polar vortex is dynamically isolated from the air outside the vortex. These conditions persist until late spring, when the vortex breaks down.

This dynamical isolation is an important prerequisite for the chemical preconditioning of the polar vortex. Air in the core of the polar vortex that has been modified by the freezing and removal of water and nitric acid during the cold Antarctic winter retains this dehydrated and denitrified character when the Sun returns to the polar region in springtime. This modified air provides the environment in which the catalytic destruction of ozone by chlorine chemistry can proceed at a rapid rate.

In this paper we calculate the potential vorticity distribution on potential temperature surfaces, using data collected by the ER-2 aircraft. Potential vorticity on isentropic surfaces is conserved for time scales of several weeks or more in the lower stratosphere and is the most fundamental characteristic of the rotational component of the flow [e.g., *Hoskins et al.*, 1986]. The aircraft data provide spatial and temporal detail that is not achievable with other measurement techniques. In principle, this resolution allows the study of fine structure in the potential vorticity distribution and offers added insight into the details of mixing processes.

Two means whereby air can be brought into the core of the polar vortex need to be considered: (1) lateral mixing and associated mean circulations produced by large-scale disturbances and (2) vertical mixing and mean circulations made possible by small-scale gravity waves. Large-scale mixing processes can be observed in potential vorticity distributions. Modeling of this large-scale mixing process has been described by *Juckes and McIntyre* [1987], and some of the consequences for the Antarctic ozone hole have been discussed by *McIntyre* [1989]. The signature of large-scale lateral mixing in process would be reversed gradients of such quantities as potential vorticity and long-lived tracers, like nitrous oxide. Strong meridional gradients in these quantities and infrequent observation of locally reversed gradients would be evidence of weak lateral mixing by large-scale disturbances. Gravity waves can produce vertical mixing by generating turbulent mixing in the process of breaking. Vertical mixing is unlikely to represent a significant source of extraneous air for the polar vortex because of the depth of the vortex relative to the mixing depth of gravity waves in the strongly stratified lower stratosphere.

At the same time gravity waves break into turbulence,

[1]Department of Atmospheric Sciences, University of Washington, Seattle.
[2]NASA Ames Research Center, Moffett Field, California.
[3]Jet Propulsion Laboratory, Pasadena, California.
[4]Laboratory for Atmospheres, NASA Goddard Space Flight Center, Greenbelt, Maryland.

Copyright 1989 by the American Geophysical Union.

Paper number 89JD00431.
0148-0227/89/89JD-00431$05.00

they may introduce a momentum change to the mean flow [e.g., *Lindzen*, 1981]. A strongly negative westerly momentum change, such as might be associated with a large-amplitude mountain wave, would cause the air parcels affected to move slightly poleward in the process of coming into geostrophic balance. If the net effect of all of the breaking gravity waves is a significant drag on the zonal mean flow, then a meridional mean flow will develop and carry constituents poleward. It is unlikely that a very large poleward mean flow is produced by gravity waves in the south polar lower stratosphere, or the polar region would be warmed by the required polar subsidence at altitudes below the wave-breaking altitude. Since, except for South America and Antarctica itself, the high-latitude southern hemisphere surface is almost entirely ocean, we expect zonally averaged mountain wave drag on the lower stratosphere to be very weak compared to the northern hemisphere. To verify this expectation, it would be useful to have quantitative estimates of the vertical flux of momentum in gravity waves averaged over latitude belts in the two hemispheres. We will not attempt a quantitative evaluation of momentum fluxes here.

Strong potential vorticity and N_2O gradients in the vicinity of strongest zonal winds confirm the relative weakness of meridional mixing processes during the period when the ozone decline is observed over Antarctica. At a particular longitude these gradients wax and wane together, as the vortex undergoes zonally asymmetric perturbations associated with large-scale waves [*Schoeberl et al.*, 1989]. On the inner edge of this region of strong potential vorticity gradient, narrow regions with weak, or even reversed, potential vorticity and N_2O gradients are occasionally observed. The relative rarity of reversals in the large-scale meridional gradients of potential vorticity and nitrous oxide and the consistent appearance of a region of strong meridional gradients in these quantities equatorward of the chemically perturbed region (CPR) suggest that mixing and mean circulation transport into the CPR is weak. This conclusion is consistent with the lack of temporal change in conservative trace gases during September 1987 and other arguments presented by *Hartmann et al.* [1989] that the effect of mass transport on the CPR is relatively small.

2. Data and Potential Vorticity Calculation

We approximate potential vorticity on potential temperature (θ) surfaces by assuming in the calculation of the planetary contribution to the vorticity that θ surfaces are approximately perpendicular to the local vertical.

$$P = -\frac{\partial \theta}{\partial p}(\zeta + f) \tag{1}$$

Where T is temperature, p is pressure, $\theta = T(p_0/p)^\kappa$ is the potential temperature, and $f = 2\Omega \sin \phi$ is the Coriolis parameter ($\kappa = R/c_p = 0.288$; $p_0 = 10^5$Pa). The relative vorticity is given in spherical coordinates by

$$\zeta = \frac{1}{a \cos \phi}\left(\frac{\partial v}{\partial \lambda} - \frac{\partial(\cos \phi\, u)}{\partial \phi}\right) \tag{2}$$

where the horizontal derivatives are taken along constant θ surfaces. The full spherical form involving latitude (ϕ) and longitude (λ) has been used in the calculations, but for brevity we can use local Cartesian coordinates to refer to the terms in the relative vorticity, as follows:

$$\zeta = \frac{\partial v}{\partial x} - \frac{\partial u}{\partial y} \tag{3}$$

The static stability can be expressed in terms of the vertical gradient of temperature in the following form, where hydrostatic balance has been assumed:

$$-\frac{\partial \theta}{\partial p} = \left(\frac{p_0}{p}\right)^\kappa \frac{T}{p}\left(\frac{R}{g}\frac{\partial T}{\partial z} + \kappa\right) \tag{4}$$

In order to calculate potential vorticity, measurements of temperature, pressure, wind velocity, and lapse rate are needed. Temperature, pressure, and wind velocity are available from the Meteorological Measurement System (MMS) aboard the ER-2. The instrumentation has been described by S. G. Scott et al. (personal communication, 1988) and the wind measurements from the AAOE have been described by *Chan et al.* [this issue]. The Microwave Temperature Profiler (MTP) on the ER-2 provides several estimates of lapse rate, as described by *Gary* [this issue]. We have used the channel 1 estimate of lapse rate, which provides an estimate for a layer about 3 km deep at flight altitude. This average of the lapse rate over a relatively deep layer is consistent with the smoothing in the meridional direction that will be applied to the data. The effective resolution will be about 3 km in the vertical and 3° of latitude, roughly in accord with the $\Delta x \sim \Delta z \cdot N/f$ scaling for Rossby waves suggested by *Juckes and McIntyre* [1987]. Thus the ratio of meridonal to vertical resolution is consistent with a search for potential vorticity features in a stratified flow, although the absolute magnitude of the resolution is set by practical, rather than theoretical considerations.

In calculating the relative vorticity, spatial information for calculating the necessary spatial gradients is available only along the flight track. Since the flight tracks are principally meridional, we can only estimate gradients in the north–south direction. In effect, we must neglect $\partial v/\partial x$ compared to $\partial u/\partial y$ in the calculation of relative vorticity. We can also think of the measurements as being taken in a natural coordinate system, where one axis is parallel to the flow and the other is perpendicular to it [*Holton*, 1979]. In this coordinate system the relative vorticity is written as in (5):

$$\zeta = -\frac{\partial V}{\partial n} + \frac{V}{R_S} \tag{5}$$

Here V is the wind speed, n is distance in a direction normal to the flow, and R_S is the radius of curvature of the streamline. The first term on the right-hand side in (5) may be called the shear vorticity, and the second term is the curvature vorticity associated with the curvature of the streamlines of the flow field. The shear vorticity can be calculated with good accuracy from the ER-2 data because the flight tracks are approximately normal to the flow direction. Since the ER-2 provides only a one-dimensional view through the flow field, the curvature vorticity cannot be directly measured. In presenting the vorticities from the ER-2 shown in this paper, we must explicitly assume that the curvature vorticity is negligible. This assumption can be tested for the large-scale component of the flow by comparing the shear and curvature vorticities along the flight track calculated from geostrophic wind fields analyzed by the National Meteorological Center (NMC). Such comparisons have been carried out. They show that the curvature term is,

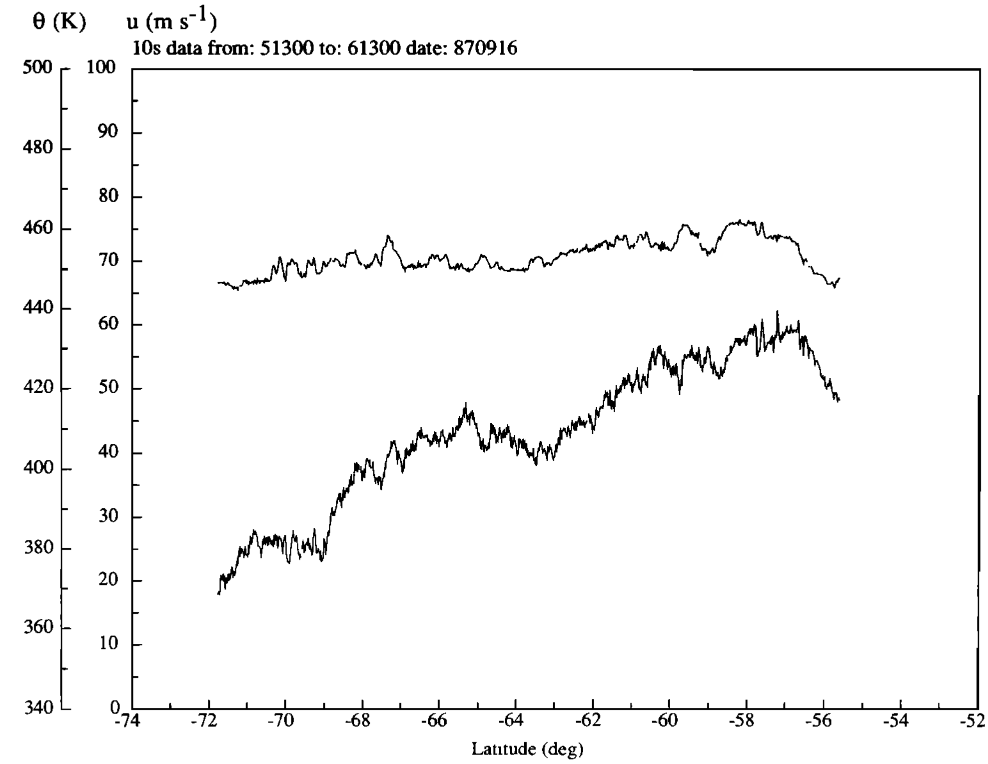

Fig. 1. Line plots versus latitude of 10-s average data from the level portion (relatively constant θ) of the southbound leg of the ER-2 flight of September 16, 1987. The upper curve and leftmost scale are potential temperature in degrees Kelvin. The lower curve and rightmost ordinate scale are for the eastward component of wind velocity in meters per second.

in fact, not negligible. Because the curvature term estimated from the NMC data remains relatively constant over the latitude band of interest, however, the curvature term tends to add a large-scale bias to the potential vorticity, rather than spatial detail. It is difficult to fully resolve this issue with coarse two-dimensional data from NMC analyses and fine one-dimensional data from the ER-2. A series of coordinated flights by two ER-2 aircraft would help define the fine spatial structure of disturbances in the stratosphere.

The data from the ER-2 provide a one-dimensional cut of very high spatial resolution through fields of temperature and velocity that are evolving in space and time. A broad range of spatial and time scales are represented in these data, from the largest scales of motion seen on hemispheric synoptic maps to rapidly evolving gravity waves and turbulence that can only be observed at these altitudes from aircraft. From the data we can only define the spatial scale along the flight path. The temporal development and three-dimensional structure of the features are not resolved. It is not clear which features should be included in evaluating the potential vorticity because of the limitations imposed by the spatial and temporal sampling and the mix of rotational and gravity wave motions contributing to the raw observations.

When we calculate potential vorticity, we will simply smooth out a lot of the detail in the data and calculate the potential vorticity that is consistent with these smoothed fields. This gives the gross structure of the potential vorticity field, which can be compared with the gross structure of the N_2O field measured by the ATLAS instrument [*Loewenstein et al.*, this issue; *Podolske et al.*, 1989]. These gross features give some indication of the overall potential vorticity distribution and its association with N_2O. Since both potential vorticity and N_2O are long-lived trace quantities in the lower stratosphere, we expect the major features of their distributions to be similar. What this approach does not allow us to do is to establish the fine-scale structure we expect to see resulting from the cascade of potential vorticity to ever smaller scales [e.g., *Juckes and McIntyre*, 1987; *McIntyre*, 1989]. It is very difficult to separate fine structure in the data that might have resulted from vorticity cascade from the fine structure associated with gravity waves, and we have not attempted that here.

3. Smoothed Profiles of Potential Vorticity

In evaluating the horizontal derivatives in (2) it is assumed that they are taken on potential temperature (θ) surfaces and that the static stability in (1) and (4) is also evaluated at a constant potential temperature level. Since static stability, in particular, varies rapidly with pressure, as can be seen from (4), it is important that the data be along an approximately constant θ surface. On most flights an attempt was made to fly the plane along constant θ surfaces between Punta Arenas and the dive and climb at the southernmost extent of the flight and then on the return flight. In calculating the potential vorticity from the flight data, it is necessary to cut the periods of rapid climb and descent at the ends of the flight to avoid contamination of the results by vertical gradients of potential vorticity or N_2O. Of course, the conservation of potential vorticity applies to potential temperature surfaces, and the relation between strong potential vorticity gradients and the lack of transport applies only to potential vorticity gradients on θ surfaces.

An example chosen for detailed description is the outbound leg of the flight taken on September 16, 1987. The

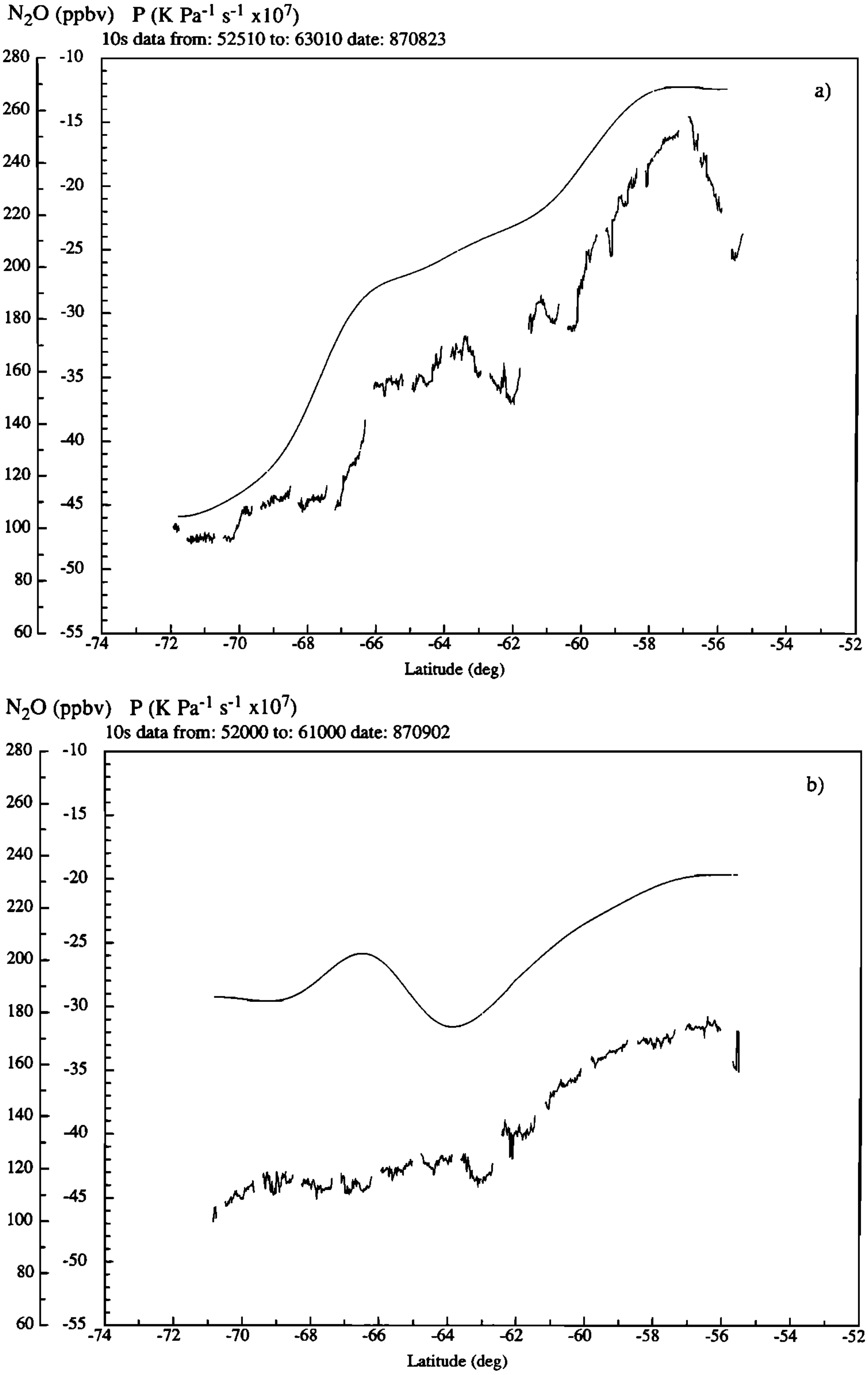

Fig. 2. Line plots versus latitude of 10-s nitrous oxide mixing ratios in parts per billion by volume (ppbv) (wiggly curve, leftmost scale) and smoothed potential vorticity (smooth curve, right scale) potential vorticity is in KPa^{-1} s^{-1} $\times$ 10^{+7}. For the level portions of the flights of (*a*) August 23, (*b*) September 2, (*c*) September 16, (*d*) September 20, and (*e*) September 22.

potential temperature and zonal wind for the portion of the flight after the climb out of Punta Arenas and before the dive at 72°S are shown in Figure 1. It can be seen that the potential temperature varied between about 460 K at the northern extremity of the flight segment and 450 K at the southern extremity, with a gradual descent marked by many small oscillations in between.

The zonal wind generally decreases toward the pole but shows a rather sharp minimum around 63°S. Potential vorticity variations at a particular latitude are largely deter-

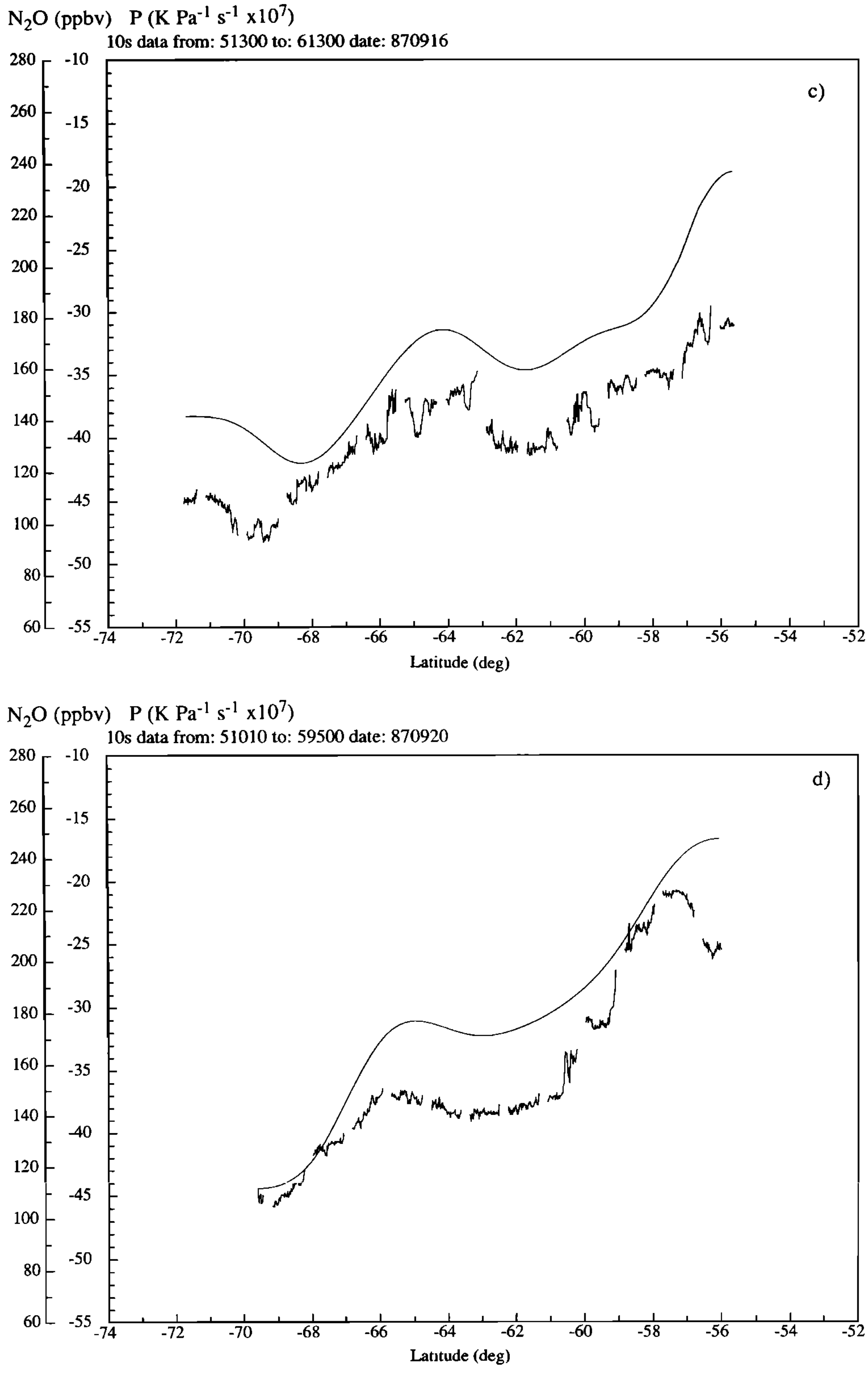

Fig. 2. (continued)

mined by the relative vorticity, with somewhat smaller contributions from lapse rate variations. From (4) we can see that the relative vorticity is related directly to the wind shear. When the wind decreases toward the pole, the relative vorticity is of the same sign as the planetary vorticity (cyclonic), and the potential vorticity is of large magnitude. Zonal wind speed increasing toward the pole is indicative of air with potential vorticity characteristic of a more equatorward latitude, while zonal wind speed decreasing toward the pole is indicative of potential vorticity with values from higher latitudes. Thus changes in sign of the meridional shear of the wind that occur in association with a zonal wind speed maximum are associated with strong enhancements of the meridional gradient of potential vorticity above the gradient implied by the variation of the Coriolis parameter. In the absence of substantial compensating changes in static stabil-

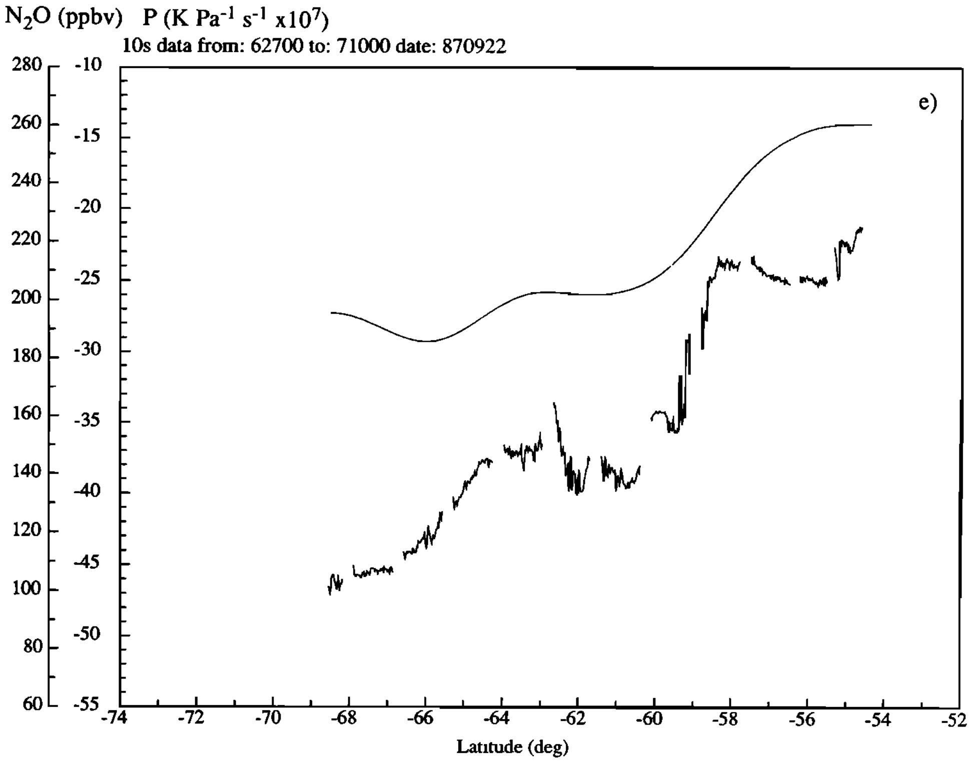

Fig. 2. (continued)

ity, the rapid change in shear near 63°S on September 16 indicates that air with potential vorticity characteristics of equatorward latitudes has intruded to the poleward side of air with more poleward characteristics. This inference is supported by the potential vorticity and N_2O plots shown in Figure 2*c*.

In order to calculate the potential vorticity from the winds, temperatures, and pressures along the flight track, most of the high-frequency variability must be removed. We believe that much of this high-frequency variability is associated with gravity waves and other fine-scale structure, which may give a false potential vorticity signature. These small-scale, gravity wave variations are discussed further in section 4. In this section we describe potential vorticity distributions calculated for data from which these high-frequency features have been removed with a digital filter.

Since we would like to retain as much of the level portion of the flight as possible, we have used multiple applications of a 1–2–1 smoother of the form

$$\hat{f}(t_i) = 0.25[f(t_{i-1}) + f(t_{i+1})] + 0.5\, f(t_i) \qquad 2 < i < N - 1$$

Here each time, t_i corresponds to a 10-s average of the data. These averages were taken before the analysis was begun. We applied equal weights to the two points on each end to determine smoothed values for the endpoints:

$$\hat{f}(t_1) = 0.5[f(t_1) + f(t_2)] \qquad \hat{f}(t_N) = 0.5[f(t_{N-1}) + f(t_N)]$$

In this way, no data are lost to the smoothing process, but we must acknowledge some overweighting of the endpoints in the resulting smoothed series. This 1–2–1 filter is applied 1000 times to all of the data used in the calculation of potential vorticity. After the meridional derivative of the

TABLE 1. Potential Temperatures of Relatively Level Portions of Flight Legs for Each of the Flights during AAOE

	Potential Temperatures, K	
Flight Date	Southbound	Northbound
August 17	420*	420*
August 18	430	425–470 (CC)
August 23	420 → 440 ~ 67°S	360–500 (CC)
August 28	425	420
August 30	425	425
September 2	425	425
September 4	425	425
September 9	450	420 (turned at 69°S)
September 16	450	420
September 20	445	440–500 (CC)
September 21	455	425
September 22	455*	430*

CC stands for cruise climb between the potential temperatures indicated; the flight was not level.
*Indicates a higher than average degree of variation in the potential temperature of flight level.

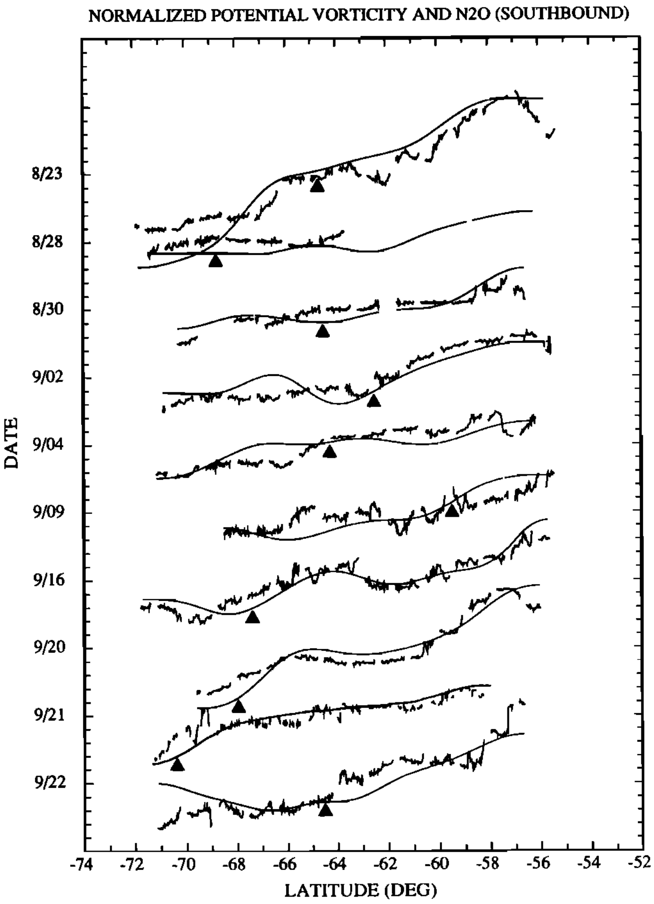

Fig. 3. Plots of normalized potential vorticity (smooth curves) and normalized nitrous oxide for the southbound portions of each flight, excluding the climb and dive. Normalization is performed by dividing each value by the mean along the flight section shown. Each day is offset by half a normalized unit, with the mean value aligned with the date indicated for the flight on the left. Triangles indicate the latitude where ClO reaches 130 pptv, which is taken to be the boundary of the chemically perturbed region overlying the pole.

zonal wind was taken to estimate the relative vorticity and the stability was multiplied times the absolute vorticity to yield the potential vorticity, the filter was again applied 10,000 times to the potential vorticity to produce the smoothed plots of potential vorticity shown in this paper. According to arguments put forward by *Haynes and McIntyre* [1987], the smoothing should be done prior to the calculation of potential vorticity, rather than afterward. In the case at hand, it makes little difference in the final field when the averaging is done, and it is more efficient to do the majority of the smoothing at the end of the process. It is not obvious what amount of smoothing should be applied to the data and the resulting potential vorticity. We have simply continued smoothing until the scale of the features remaining in the potential vorticity was of the order of a few degrees of latitude. At this point a good correspondence appears between the scale of the features remaining in the potential vorticity and those apparent in the unsmoothed N_2O plots.

We would very much have liked to search for the fine structure in the potential vorticity field that is postulated to result from large-scale waves contorting the potential vorticity distribution, as suggested by *Juckes and McIntyre* [1987] and *McIntyre* [1989]. The problem to be overcome is that the scale of these features becomes similar to that of gravity wave features and it is difficult to disentangle fine structure produced by large-scale waves from that associated with gravity waves. Indeed, it seems probable that rapidly evolving scale changes associated with Rossby-wave breaking is a significant source of gravity wave motions. Furthermore, breaking gravity waves can force rotational flows. It must therefore be that an intermediate scale exists where gravity wave and rotational flows are not physically or logically separable.

A fair degree of agreement exists between the shape of the N_2O structure and the potential vorticity structure, as is shown in Figures 2*a*–2*e*. All of the data shown in Figure 2 are for the southbound portions of the flights for the days shown, except for the flight on September 22, which is the northbound leg. On August 23 the flight path increased significantly in potential temperature, from 420 to 440 K between 66° and 67°S, which explains much of the jump in both potential vorticity and N_2O at that latitude. The flight of September 2 was not at a particularly constant θ, varying between 415 and 435 K, but the variations do not strongly affect the interpretation of the smoothed potential vorticity on that day. The rest of the flight portions shown were at relatively constant potential temperatures of about 430 K for September 22 and 450 K for September 16 and 20 (Table 1).

The flight days shown in Figure 2 are those with the most dramatic variations in N_2O and potential vorticity associated with interesting dynamical structure. That similar features are present in both of these quantities is consistent with the idea that since they are both conservative on relatively long time scales, structures resulting from deformations along θ

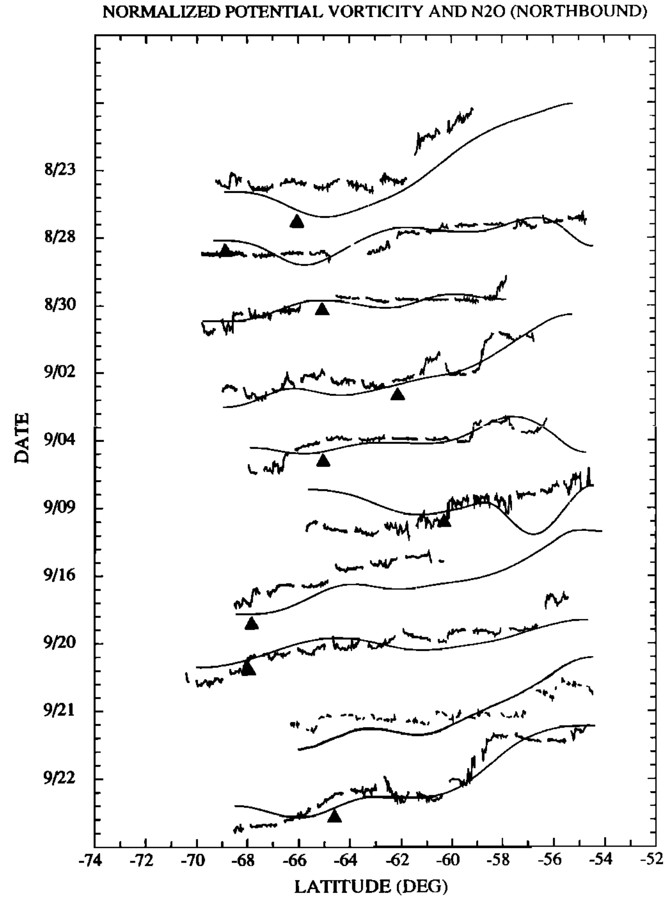

Fig. 4. Same as Figure 3, except for the northbound flight legs.

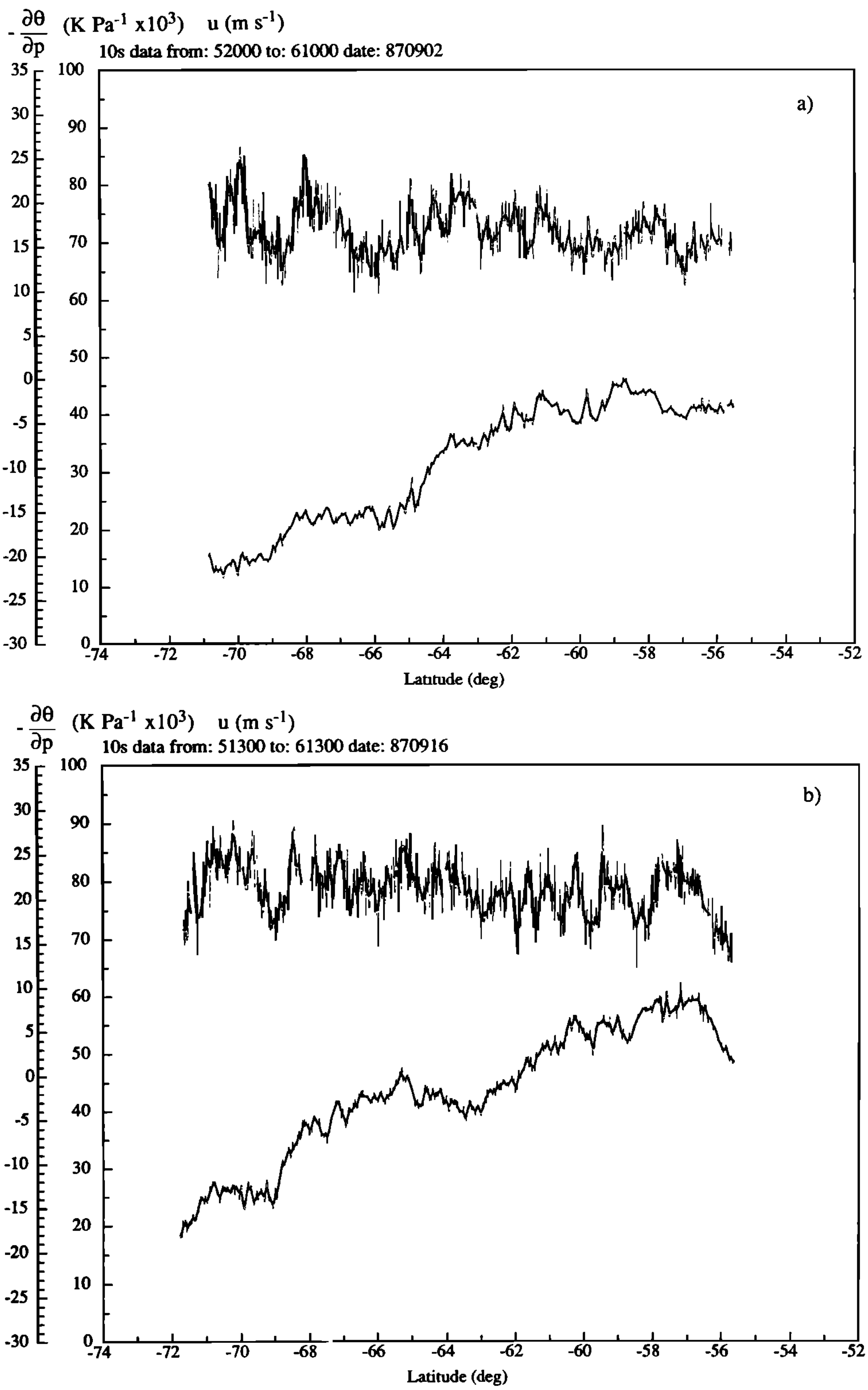

Fig. 5. Line plot versus latitude of static stability, $-\partial\theta/\partial p$, (left scale, KPa^{-1} $\times$ 1000) and eastward component of wind (right scale, m s^{-1}) for the southbound legs of (*a*) September 2, (*b*) September 16, and (*c*) September 22. The raw 10-s data are shown as a light curve and slightly smoothed data are shown as a heavier curve.

surfaces occurring on relatively short time scales should produce similar features in both quantities.

Not all flight days had dramatic features in the N_2O and potential vorticity. The collections of southbound and northbound legs on all flight days are shown in Figures 3 and 4, respectively. Both the potential vorticity and N_2O have been normalized by dividing by the mean along the flight track to take out variations associated with the differing mean potential temperatures of the flight tracks. Not all of these flight tracks were at constant θ. The meridional gradient and the

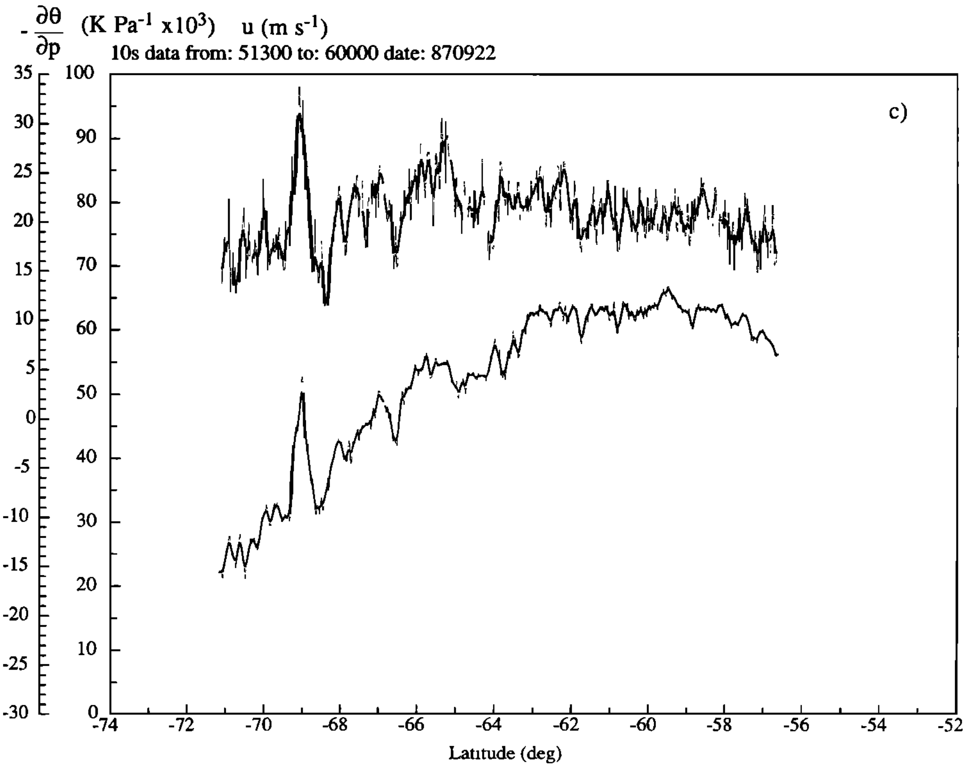

Figure 5. (continued)

amount of small-scale variability of the N_2O and potential vorticity vary from flight to flight. On some days the meridional gradient is steep in association with a concentrated jet stream, and on other days the gradients are very weak. Changes like this are expected in association with the movement and changing amplitudes of synoptic- and planetary-scale meteorological disturbances. The evolution of the synoptic structure and its association with the constituent concentrations has been described by *Schoeberl et al.* [1989]

Figures 3 and 4 indicate that reversals of the meridional gradients of potential vorticity and N_2O on spatial scales that are greater than a couple of degrees occur very rarely, perhaps only for the southbound leg of the flight of September 16. A lack of gradient reversals suggests that large-scale lateral mixing is a relatively rare event during this season at this location. Such a conclusion is consistent with the weakness of the Eliassen-Palm (E-P) flux divergence in the lower stratosphere around Antarctica during September [*Mechoso et al.* 1985].

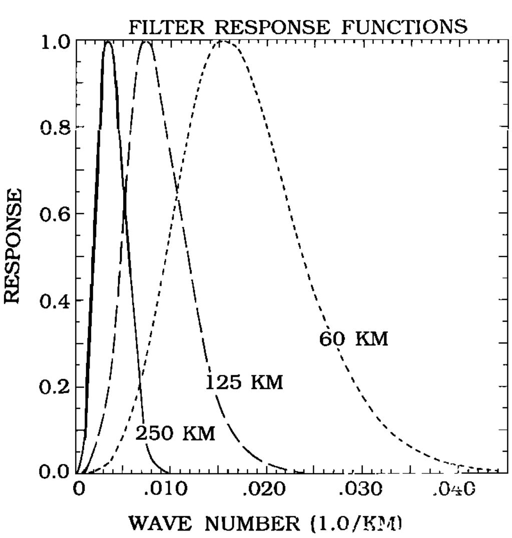

Fig. 6. Response functions for the numerical filters used to isolate small-scale features. The wave number scale was constructed from a frequency scale, using the mean meridional ground speed of the ER-2.

4. Small-Scale Structures and Correlations

It has been assumed to this point that variations in wind and static stability with meridional wavelengths of less than a few degrees are contributed primarily by gravity wave motions. In this section we support this assertion with calculations of the lag correlations between zonal wind speed, relative vorticity, and static stability measured along the level portions of the flight tracks. Examples of the static stability and zonal wind measurements are shown for the southbound flights of September 2, 16, and 22 in Figure 5. Very strong features in both zonal wind speed and static stability associated with a large gravity wave appear near 69°S on September 22. A strong enhancement in static stability is associated with a similarly dramatic increase in zonal wind speed. Similar, though less dramatic, features in static stability and zonal wind that appear related to one another are evident on the other days shown.

To quantify these relationships in an objective way, we perform lag correlations between the zonal wind speed and the static stability and between the relative vorticity and the static stability. In order to isolate particular spatial scales, we band-pass filter the data before performing the correlations. Three band-pass filters are used, whose response functions are shown in Figure 6. These response functions

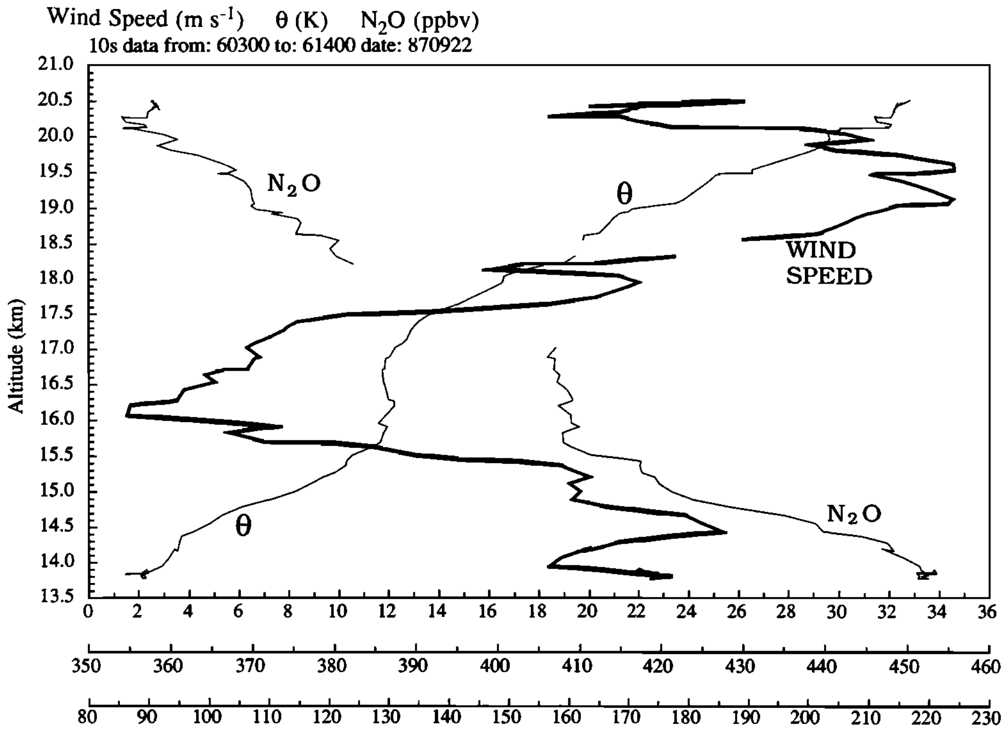

Fig. 7. Vertical profiles of wind speed (heavy curve, top scale in m s^{-1}), potential temperature (middle scale, °K), and nitrous oxide (bottom scale, ppbv) for the dive portion of the flight of September 22.

are peaked at wavelengths of about 60, 125, and 250 km and are constructed by using multiple applications of the 1–2–1 filter described in section 2. The 60-km filter is obtained by subtracting the 10-s average data smoothed 200 times with the 1–2–1 filter from the data smoothed 50 times. The 125-km wavelength filter is 200 smoothings minus 1000 smoothings, and the 250-km filter is 1000 smoothings minus 5000 smoothings. An average ground speed for the aircraft is used to translate frequency into meridional wavelength.

Absolute vorticity, as defined here, is negative in the southern hemisphere, so that positive relative vorticity deviations result in a reduction in the magnitude of the absolute vorticity. Static stability, defined as $-\partial\theta/\partial p$, is positive for a stable atmosphere. If the motions are potential vorticity conserving and the potential vorticity variations are smaller than the individual variations in static stability and relative vorticity, we expect a positive correlation between relative vorticity and static stability, so that the combined product of static stability and absolute vorticity will remain relatively constant.

For gravity wave motions, which we do not expect to yield a potential vorticity–conserving signature in the data, the expected correlation between wind speed and static stability is less straightforward to determine. The expected correlation can be easily calculated for linear waves propagating in a mean state, with uniform mean wind and mean static stability. If we assume a harmonic solution and two-dimensional flow in the x-z plane, a relationship between static stability and wind speed can be derived,

$$\frac{\partial\theta'}{\partial z} = (\bar{u} - c)(m^2 + k^2)\,\frac{\bar{\theta}}{g}\,u' \tag{6}$$

where z is height, m and k are the vertical and zonal wave numbers, respectively, u is the zonal wind, θ is potential temperature, g is the acceleration of gravity, and c is the phase speed in the zonal direction. Overbars and primes represent mean and perturbation values, respectively, in the linear perturbation expansion. This relationship (6) shows that for linear gravity waves, zonal wind and static stability variations should be in phase if the mean zonal wind is greater than the phase speed. A strong positive correlation between zonal wind and static stability is certainly evident in the mountain wave event on the flight of September 22 (Figure 5c).

If gravity waves are in the process of breaking, then it is difficult to say what correlation between static stability and zonal wind should be expected. It is presumed that this process is rather quick but is probably also associated with large amplitudes, so that waves in the process of breaking may be infrequently observed but still give a significant contribution to the calculated correlations. If the waves have completely broken down and left their mark on the mean flow, we expect a region with decreased static stability caused by vertical mixing to be associated with a momentum anomaly, whose sign would depend on the phase speed of the wave that has been absorbed. If we assume that the breaking waves are principally mountain waves with nearly stationary phase, then we would expect the breaking wave to introduce a reduction in the westerly wind of the lower stratosphere. This would give, again, a positive correlation between static stability and zonal wind speed.

A classic example of mountain wave propagation and breaking was observed on the dive portion of the flight of September 22. The ER-2 performed a steep dive, beginning at about 72°S, just downstream of Alexander Island. Alexander Island possesses significant north–south oriented topography, featuring 2987-m Mount Stephenson near 70°S. Vertical profiles of potential temperature, wind speed, and

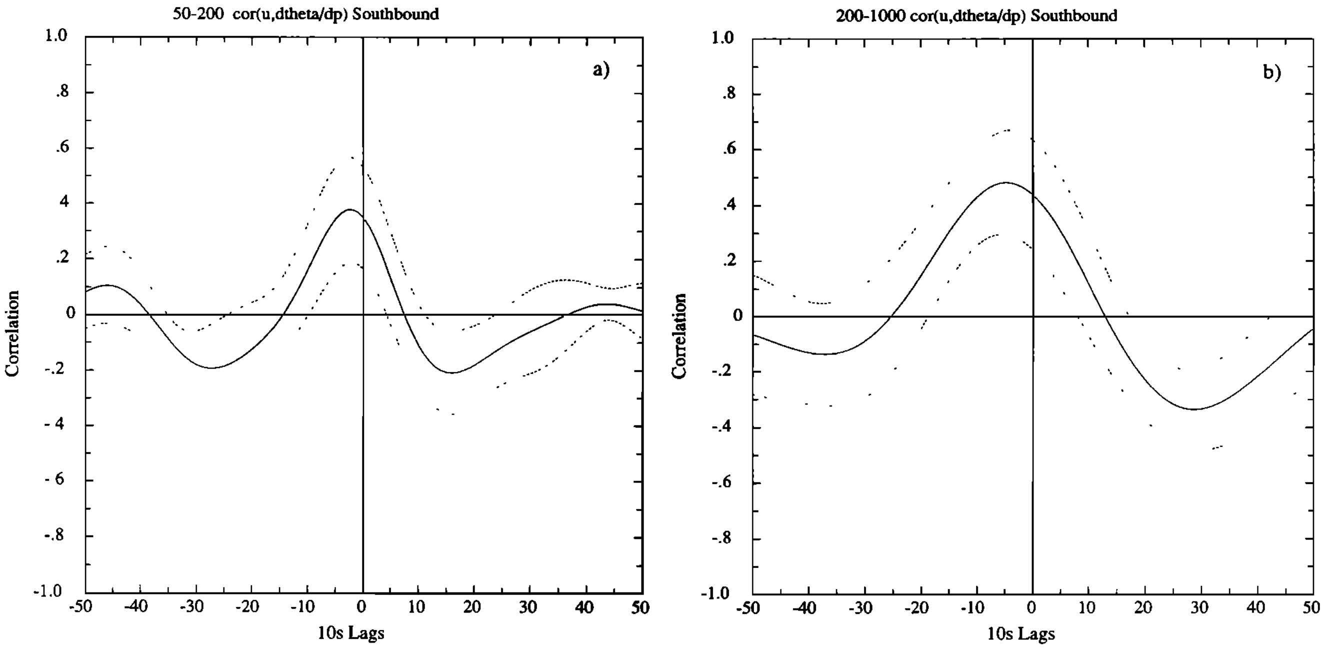

Fig. 8. Lag correlation between zonal wind speed and static stability. Positive lags indicate that the static stability is to the south of the wind perturbation. Lag numbers indicate 10-s intervals of flight time. (*a*) A 60-km wavelength band pass, (*b*) 125-km filter, and (*c*) 250-km filter. Dashed lines indicate 95% confidence limits.

nitrous oxide are shown in Figure 7. In a 2-km-thick layer between 15.5 and 17.5 km (pressure altitude), the wind speed falls from around 20 m s^{-1} to near zero. In the same altitude range, both the potential temperature and N_2O are well mixed. This is the clear signature of a mountain gravity wave that has attained large amplitude and broken. Below this layer of well-mixed and momentum-depleted air, we see a smaller gravity wave. We observe first weak wind speeds at about 14 km, associated with weak static stability, as (6) predicted. At 14.5 km the wind and the static stability are stronger. This wave appears to be approaching the breaking stage. Since the dive took place at 72°S, the large gravity wave shown in Figure 7 is presumably not the same one seen near 69°S in Figure 5*c*. The two events also appear at significantly different potential temperatures, near 455 K in Figure 5*c* and near 390 K in Figure 7.

The calculated lag correlation functions for the three filters, together with 95% confidence limits, are shown in Figure 8. These show the correlations between wind speed and static stability, averaged for the level portions of the southbound legs of the last 10 flights except for that of August 30, which has a significant gap. In accord with expectations for both the linear and the fully absorbed westward propagating gravity wave, the correlations between static stability and zonal wind along the flight legs are positive. The consistency from flight to flight of the positive correlations at zero lag are indicated in Table 2. The average correlations are not exceedingly large, peaking at only about 0.4. The reasons for the low correlations may include the fact that not all waves propagate westward relative to the mean flow. For eastward propagating linear gravity waves we expect a negative correlation between static stability and wind, according to (6). Similarly, when waves with eastward intrinsic phase speeds have been absorbed into the flow, we expect positive westerly wind anomalies in association with weak static stability. In addition, the measurements themselves may underestimate the true correlations. The remote-sensing measurement of lapse rate from the MTP is for a layer about 3-km deep, and the wavelength of the operative gravity waves may vary considerably, as is evident in Figure 7.

The maximum correlations are displaced somewhat in latitude, with the zonal wind being best correlated with static stability variations about one twelfth of a wavelength to the north. It follows that the relative vorticity variations are best correlated with static stability variations about one sixth of a wavelength to the south (calculated but not shown here). These phase variations seem to be independent of the meridional wavelength of the disturbance, within the range

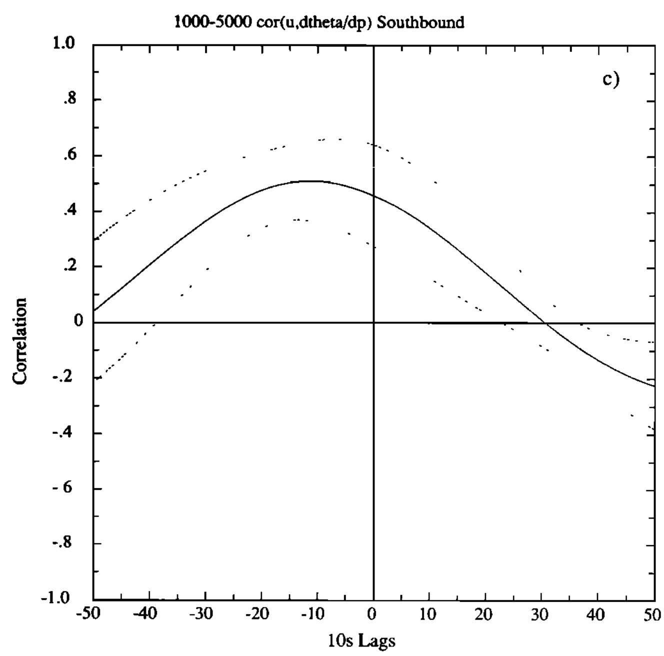

Fig. 8 (continued)

TABLE 2. Correlation of u and $-\partial\theta/\partial p$ at Zero Lag Along Level Portion of Flight Track on Each of Days Shown

Band	Aug. 23, 1987	Aug. 28, 1987	Sept. 2, 1987	Sept. 4, 1987	Sept. 9, 1987	Sept. 16, 1987	Sept. 20, 1987	Sept. 21, 1987	Sept. 22, 1987
Southbound									
60 km	+0.093	+0.268	+0.394	+0.566	+0.166	+0.312	+0.439	+0.197	+0.691
125 km	+0.107	+0.332	+0.320	+0.412	+0.330	+0.584	+0.425	+0.567	+0.843
250 km	+0.345	+0.231	+0.529	+0.293	+0.437	+0.673	+0.265	+0.556	+0.791
Northbound									
60 km	+0.370	+0.379	+0.393	+0.248	+0.406	+0.271		+0.020	+0.299
125 km	+0.307	+0.261	+0.544	+0.357	+0.229	+0.335		+0.175	+0.450
250 km	+0.377	+0.478	+0.814	+0.687	+0.696	+0.492		+0.243	+0.421

of 60–250 km shown in Figure 6. Similar results were found for the northbound flight tracks (not shown). An additional complication is introduced by the fact that the gravity waves are not approximately two dimensional. The phase shift may be related to the adjustment of the flow to localized wave breaking [e.g., *Zhu and Holton*, 1987]. When waves of limited horizontal extent affect the momentum balance locally, vertical and meridional circulations are generated that act to bring the flow back into geostrophic balance. These circulations will cause additional adjustments of zonal wind and static stability.

5. Relationship to the Chemically Perturbed Region

The photochemical theories for the ozone hole involve removal of odd nitrogen species and water from the polar vortex, allowing a chemically perturbed region to develop where chlorine can migrate to the radical species that attack ozone. During the AAOE the core of the polar vortex was found to be low in total water [*Kelly et al.*, this issue], low in total odd nitrogen [*Fahey et al.*, 1989], and high in chlorine monoxide [*Brune et al.*, 1989; *Anderson et al.*, this issue (*a*, *b*)]. For these conditions to develop and for ozone to be removed, the chemically perturbed region must remain relatively isolated from the rest of the stratosphere. Without this isolation, water, odd nitrogen species, and heat would be transported in at too great a rate for the special conditions inside the polar vortex to be maintained.

In this section we investigate the structure of potential vorticity and nitrous oxide relative to the edge of the CPR to see if any significant features of these two tracers appear near the CPR boundary. The first objective of this exercise is to verify that the CPR is poleward of strong gradients of potential vorticity. This would show that the CPR is within a band of latitudes where meridional mixing on θ surfaces is weak. The second purpose is to look for evidence that the strong change in ozone concentration across the CPR boundary might be inducing dynamical changes. Ozone is the principal absorber of solar radiation in the stratosphere, so that the sharp decrease in ozone concentration from the equatorward to the poleward side of the CPR may lead to radiatively induced dynamical features. This is an important consideration, since the sense of the radiatively induced changes is to reduce the solar heating of the core of the polar vortex. *Shine* [1986] calculated a net cooling due to the ozone depletion of about 0.4 K day^{-1} at 20 km, which resulted principally from reduced absorption of solar radiation by ozone. This reduced heating would cause the intense vortex and cold temperatures over the pole to persist longer into the spring season [e.g., *Kiehl et al.*, 1988] and thereby prolong the time period or areal extent of ozone destruction by chlorine photochemistry.

The boundary of the CPR is defined as the point where the ClO first rises significantly above the background. Following *Proffitt et al.* [this issue], we have arbitrarily chosen 130 parts per trillion by volume (pptv) to mark the boundary of the CPR. The latitudes of the boundary of the CPR determined with this definition are indicated in Figures 3 and 4 with triangles. To determine an average structure relative to the boundary of the CPR, data from all flights beginning with the flight of August 23, 1987, have been composited in latitude coordinates relative to the CPR boundary. Compositing has been done separately for data falling between 415 and 435 K and between 440 and 460 K, nominally the 425 K (~75 mbar) and 450 K (~60 mbar) surfaces, respectively.

The wind, potential vorticity, nitrous oxide, and ozone structure relative to the CPR boundary at the 425 K level are shown in Figure 9. The ozone data are described further by *Starr and Vedder* [this issue]. The CPR boundary is about 5° of latitude poleward of the core of maximum wind speeds and poleward of the latitudes with the strongest meridional gradient of potential vorticity. The strongest meridional gradients of both potential vorticity and nitrous oxide are equatorward of the CPR boundary, and the gradients appear to weaken slightly inside of the boundary. Ozone changes sharply across the CPR boundary. The composite ozone profile increases again at its most poleward extent, but this feature is not considered to be statistically significant. Only a few of the flights penetrated as much as 6° into the CPR and these were mostly before September 16, the date of the first flight for which the ozone hole was fully developed. There is in addition an increase in the composite potential temperature from 422 to 431 K between −4° to −7° of relative latitude, which contributes to the apparent increase of ozone with latitude.

At the 450 K level the CPR boundary appears to be at the inner edge of the region of strongest winds (Figure 10). The composite potential vorticity appears to undergo a sharp drop in the vicinity of the CPR boundary, although the 95% confidence limits on the mean vorticity profile are very wide and do not warrant rejecting a null hypothesis that the potential vorticity varies smoothly across the 20° latitude range pictured. The composite nitrous oxide profile shows a similar enhancement of its meridional gradient near the CPR boundary, which is statistically significant. Weaker gradients seem to prevail both poleward and equatorward of the enhanced gradients near the CPR boundary, although significant gradients persist to the equatorward margin of the diagram.

The reality of the sharp gradient in potential vorticity near

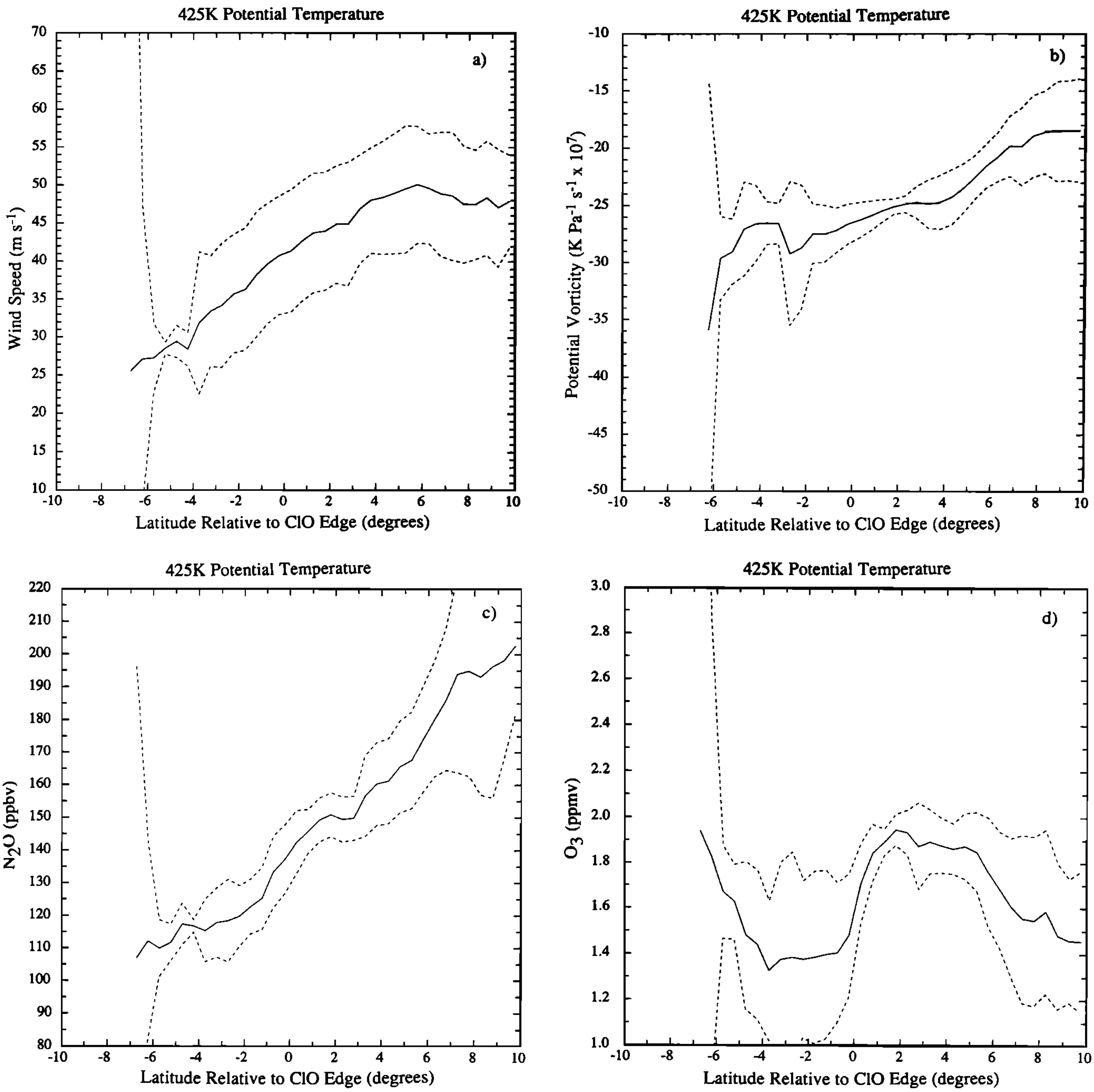

Fig. 9. Average (*a*) zonal wind, (*b*) potential vorticity, (*c*) nitrous oxide and (*d*) ozone latitude structure relative to the boundary of the chemically perturbed region, composited for all data in the range 425 ± 10 K, for flights between August 23 and September 22. Dashed curves indicate the 95% confidence limits on the mean. The south pole is toward the left, in the direction of decreasing latitude.

the CPR boundary at 450 K is as well-established as one can expect with only five flights. Table 2 shows the flight levels for the southbound and northbound portions of all of the flights. The 450 K composites come from the southbound portions of the five flights taken after September 9. Referring to Figure 3, one can see that each of these flights shows a feature indicating enhance gradients at or slightly equatorward to the CPR boundary. Corresponding features are evident in the nitrous oxide profiles. The feature is thus not contributed by one or two extreme events but occurs with about the same amplitude in each of five flights.

The question that next arises is why enhancements in the meridional gradients of potential vorticity and nitrous oxide should occur in the vicinity of the CPR boundary. It seems unlikely that the correspondence between the CPR edge and enhanced potential vorticity gradients should be caused by the effect of the dynamics on the chemistry. As has been shown here, a relatively wide region of strong potential vorticity and N_2O gradients exists on the equatorward flank of the CPR, which can act to inhibit the mixing of air from outside to inside the CPR. Therefore enhanced gradients in potential vorticity at the edge of the CPR are not necessary for its maintenance, although they would enhance the dynamical isolation of the CPR. The boundary of the CPR is presumably related primarily to the temperature history, which determines whether nitric acid or water can condense

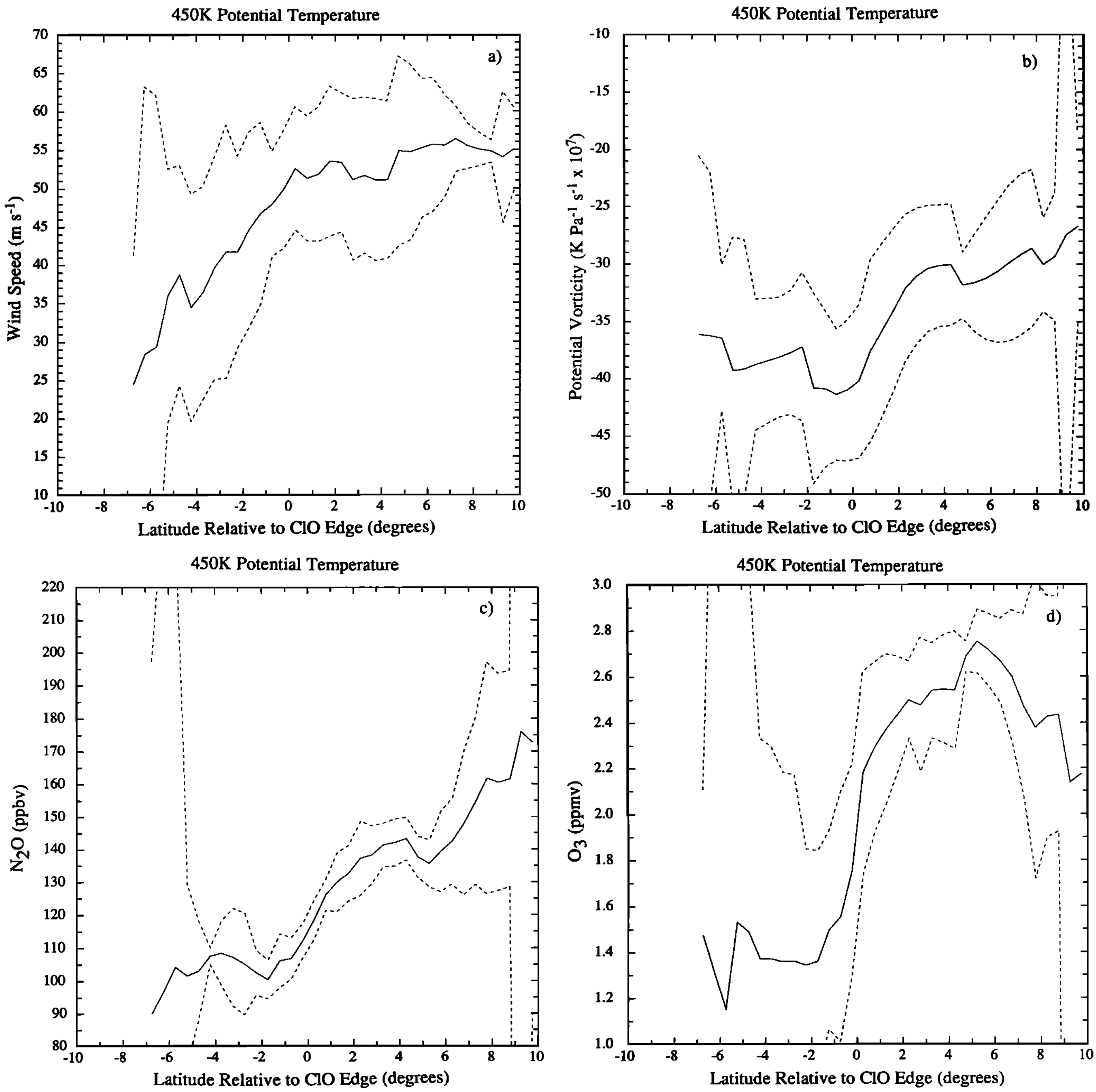

Fig. 10. Same as Figure 9, except for 450 ± 10 K.

at a particular pressure. The temperature at the CPR boundary is about 198 K in the composites for both the 425 and 450 K potential temperature surfaces (not shown).

It is more likely that the association between the CPR boundary and a narrow region of enhanced potential vorticity and nitrous oxide gradients is produced by the sharp gradient in ozone, which develops coincidently with the gradient in chlorine monoxide. At these altitudes, ozone heating is dominated by absorption in the Chappuis bands and is proportional to the ozone concentration. Therefore we expect the solar heating by ozone absorption to decrease by an amount proportional to the decrease in ozone mixing ratio, which drops by nearly 50% across a few degrees of latitude at the CPR boundary. Since the ozone heating is about 1 K day^{-1} at the 450 K level and longwave relaxation of temperature perturbations is relatively inefficient, we expect a significant dynamical response to this heating gradient, which may be what we observe in Figures 10*b* and 10*c*. *Kiehl et al.* [1988] have shown that the radiative effect of the antarctic ozone depletion leads to significant dynamical changes in a general circulation model.

Gradients in conservative quantities can also be produced by one-sided mixing processes. If lateral mixing occurs in a kind of "surf zone" of efficient mixing [*Juckes and McIntyre*, 1987] at the edge of a region of strong gradients, then even stronger gradients can be induced at the boundary between the region of strong gradient and the well-mixed surf zone. Since the N_2O gradients are strong in a region that extends well equatorward of the ClO boundary, the ClO boundary is not in contact with the mixing region on the equatorward side of the vortex wall. Indeed, it is the major thesis of this paper that the vortex wall extends well equatorward of the ClO wall and that the region of high ClO is well-insulated from intrusions of extravortical air.

Mixing on the poleward edge of the vortex wall could be the explanation for the enhanced gradients at the ClO boundary. On the poleward side of the ClO boundary we find evidence of slackened N_2O and potential vorticity gradients on θ surfaces. This would be consistent with rather efficient mixing within the core of the vortex and possible one-sided erosion of the vortex wall from the inside. This mixing would be associated with disturbances of synoptic scale which propagate poleward across the vortex wall as linear Rossby waves and then break on the poleward side or move under the vortex in the troposphere and then propagate upward. Disturbances of this type are also associated with the ozone "miniholes" discovered during the AAOE experiment [*McKenna et al.*, this issue].

It is interesting that steep gradients in potential vorticity and N_2O appear near the CPR boundary at 450 K but not at 425 K. One would expect a stronger radiative response to the ozone discontinuity to develop more at higher altitude and later in the experiment, which is consistent with the observed differences between the 425 and 450 K composites. This may be an effect of the roughly 1.5-km altitude change, but it seems more likely to result from the different temporal sampling at the two levels. To present a strong case for the potential vorticity feature at 450 K being driven by the radiative response to the ozone gradient, one would need to demonstrate that the potential vorticity gradient developed in time after the ozone gradient became established. As can be seen in Table 1, virtually all of the 450 K data come from the southbound legs of the last five flights of the experiment. At 425 K most of the deep penetrations of the CPR were made during the five flights between August 23 and September 4. The 425 K data for the last five flights came on the return leg of the flight, after a dive to lower altitudes. Because of the time required to execute the dive, the level-flight 425 K data from the last five flights do not penetrate deeply into the CPR.

By using Table 1 and Figures 3 and 4, the reader can judge whether the gradients of N_2O and potential vorticity at the CPR boundary increase with time at the 425 K level. We have composited the 425 K data separately for the two periods August 23 to September 4 and September 9–22 to test for changes. The meridional gradients of nitrous oxide and potential vorticity at the CPR boundary are somewhat greater for the composite of the latter five flights at 425 K, but the differences are not significant at the 95% confidence level. The N_2O composites for early and late in the experiment at 425 K are shown in Figure 11. While the latter half of the flights shows an enhanced gradient near the ClO boundary, the gradient is somewhat different at all latitudes, so that it is possible that the differences are a result of changing meteorology independent of any anomalous radiative forcing associated with the ozone hole.

6. CONCLUSION

Wind, temperature, pressure, and lapse rate measurements from the MMS and the MTP on the ER-2 aircraft can be used to approximate potential vorticity. Potential vorticities calculated from ER-2 flight data from AAOE compare well with the gross features of potential vorticity calculated

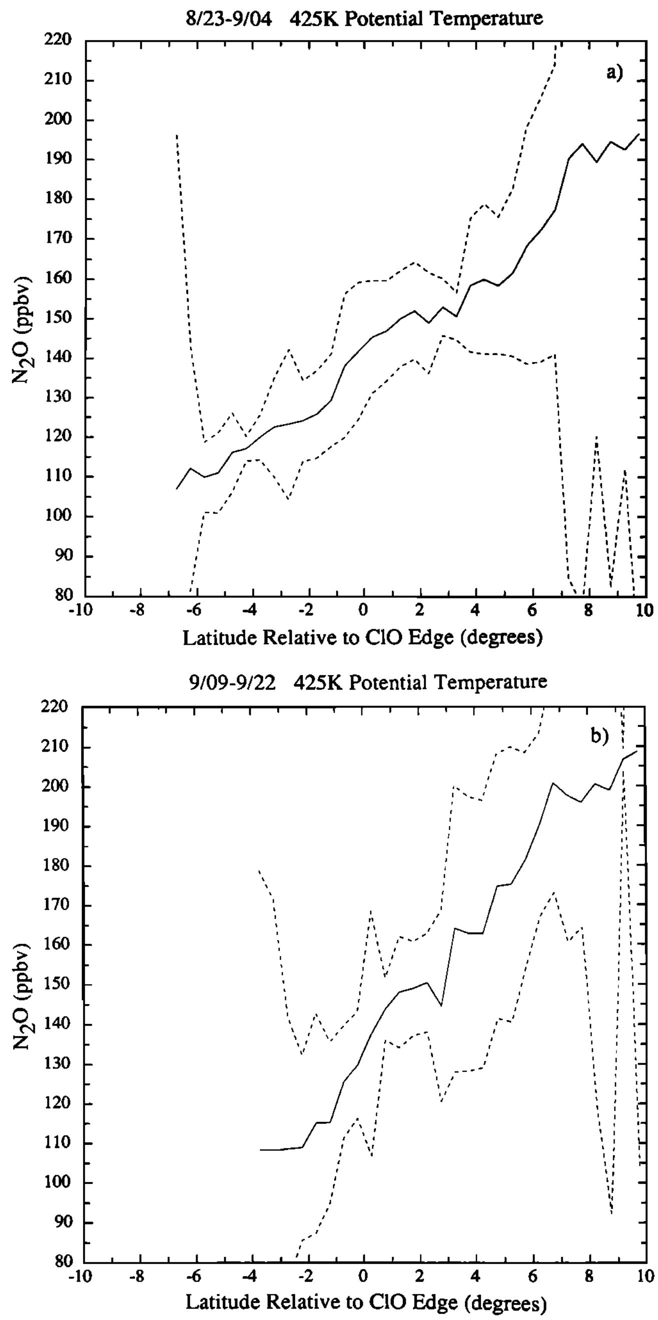

Fig. 11. N_2O composite as in Figure 9*c*, except composited for the flights between (*a*) August 23 and September 4, and (*b*) September 9 and 22.

from NMC-mapped products, and with the N_2O measurements from the ATLAS instrument on the ER-2. The flight data show substantial variations in the latitudinal distributions of potential vorticity and N_2O from flight to flight, associated with the movement of large-scale weather systems. The majority of the flights show a monotonic decrease of potential vorticity and nitrous oxide toward the pole on isentropic surfaces.

Substantial gradients in potential vorticity and N_2O exist over a finite band of latitudes equatorward of the region where the ozone depletion is occurring. This indicates that the ozone hole is isolated from extratropical air by a band of latitudes in which meridional mixing is relatively weak. Only one flight in 10, the flight of September 16, 1987, shows a significant reversal in the gradients of potential vorticity and nitrous oxide that seems likely to be associated with large-scale irreversible meridional mixing. The potential vorticity and nitrous oxide data thus indicate that large-scale meridional mixing is relatively inefficient during the month of September 1987 at the altitudes of the ozone depletion.

Fine spatial scale features in the data are contributed by gravity waves. The correlations between wind speed and static stability are as expected for gravity waves that propagate westward relative to the mean flow. Significant evidence for mountain waves and mountain wave breaking are present in the data. The meridional mixing associated with these waves is expected to be localized. Antarctica is relatively smooth, and topography is totally lacking over the middle latitudes of the southern hemisphere. If orographic gravity waves are of most importance, then the role of gravity waves in inducing mean circulations and vertical mixing in the high-latitude lower stratosphere of the southern hemisphere is expected to be relatively weak compared to the northern hemisphere. Major gravity wave breaking events were observed in the vicinity of the local topography, but the flight track followed the Palmer Peninsula, one of the few north–south oriented orographic features in the latitude band where the edge of the ozone hole appears.

Compositing of potential vorticity and nitrous oxide relative to the boundary of the chemically perturbed region showed enhanced gradients near the ClO edge. This may be a result of the sharp gradient in solar heating associated with the sharp gradient in ozone mixing ratio that developed there over the course of the experiment. This suggests direct evidence of a dynamical response to the ozone hole, which would tend to enhance the low temperatures and dynamical isolation of the polar lower stratosphere and would feed back positively on the ozone hole.

Acknowledgments. The first author would like to thank J. R. Holton and D. R. Durran for useful conversations and suggestions. Holton suggested looking at the relation between the potential vorticity and the edge of the CPR. M. E. McIntyre and the anonymous reviewers provided useful comments that improved the manuscript. Marc Michelsen and Mark Wensman performed most of the calculations and produced the figures. This work was supported by the National Aeronautics and Space Administration under grants and contracts supporting the Airborne Antarctic Ozone Experiment. We would like to thank our colleagues on the experiment team for their cooperation in producing a unique data set and for a lively exchange of ideas during the interpretive phase of the experiment.

REFERENCES

Anderson, J. G., W. H. Brune, and M. H. Proffitt, Ozone destruction by chlorine radicals within the Antarctic vortex: The spatial and temporal evolution of ClO–O_3 anticorrelation based on in situ ER-2 data, *J. Geophys. Res.*, this issue (*a*).

Anderson, J. G., W. H. Brune, S. A. Lloyd, D. W. Toohey, W. L. Starr, S. P. Sander, M. Loewenstein, and J. R. Podolske, Kinetics of O_3 destruction by ClO and BrO within the Antarctic vortex: An analysis based on in situ ER-2 data, *J. Geophys. Res.*, this issue (*b*).

Brune, W. H., J. G. Anderson, and K. R. Chan, In situ observations of ClO in the Antarctic: ER-2 aircraft results from 54° to 72°S latitude, *J. Geophys. Res.*, in press, 1989.

Chan, K. R., S. G. Scott, T. P. Bui, S. W. Bowen, and J. Day, Temperature and horizontal wind measurements on the ER-2 aircraft during the 1987 Airborne Antarctic Ozone Experiment, *J. Geophys. Res.*, this issue.

Fahey, D. W., D. M. Murphy, C. S. Eubank, K. Kelly, M. H. Proffitt, G. V. Ferry, M. K. W. Ko, M. Loewenstein, and K. R. Chan, Measurements of nitric oxide and total reactive nitrogen in the Antarctic stratosphere: Observations and chemical implications, *J. Geophys. Res.*, in press, 1989.

Gary, B. L., Observational results using the Microwave Temperature Profiler during the Airborne Antarctic Ozone Experiment., *J. Geophys. Res.*, this issue.

Hartmann, D. L., L. E. Heidt, M. Loewenstein, J. R. Podolske, J. Vedder, W. L. Starr, and S. E. Strahan, Transport into the south polar vortex in early spring, *J. Geophys. Res.*, in press, 1989.

Haynes, P. H., and M. E. McIntyre, On the representation of Rossby wave critical layers and wave breaking in zonally-truncated models, *J. Atmos. Sci.*, *44*, 2381–2404, 1987.

Holton, J. R., *An Introduction to Dynamic Meteorology*, Academic, San Diego, Calif., 1979.

Hoskins, B. J., M. E. McIntyre, and A. W. Robertson, On the use and significance of isentropic potential vorticity maps, *Q. J. R. Meteorol. Soc.*, *111*, 877–946, 1986. (Correction, *Q. J. R. Meteorol. Soc.*, *113*, 402–404, 1986.)

Juckes, M. N., and M. E. McIntyre, A high resolution, one-layer model of breaking planetary waves in the stratosphere, *Nature*, *328*, 590–596, 1987.

Kelly, K. K., et al., Dehydration in the lower Antarctic stratosphere during late winter and early spring, 1987, *J. Geophys. Res.*, this issue.

Kiehl, J. T., B. A. Boville, and B. P. Briegleb, Response of a general circulation model to a prescribed Antarctic ozone hole, *Nature*, *332*, 501–504, 1988.

Lindzen, R. S., Turbulence and stress due to gravity wave and tidal breakdown, *J. Geophys. Res.*, *86*, 9707–9714, 1981.

Loewenstein, M., J. R. Podolske, K. R. Chan, and S. E. Strahan, Nitrous oxide as a dynamical tracer in the 1987 Airborne Antarctic Ozone Experiment, *J. Geophys. Res.*, this issue.

McIntyre, M. E., On the Antarctic ozone hole, *J. Atmos. Terr. Phys.*, *51*, 29–43, 1989.

McKenna, D. S., R. L. Jones, J. Austin, E. V. Browell, M. P. McCormick, A. J. Krueger, and A. F. Tuck, Diagnostic studies of the Antarctic vortex during the 1987 Airborne Antarctic Ozone Experiment: Ozone miniholes, *J. Geophys. Res.*, this issue.

Mechoso, C. R., D. L. Hartmann, and J. D. Farrara, Climatology and interannual variability of wave, mean-flow interaction in the southern hemisphere, *J. Atmos. Sci.*, *42*, 2189–2206, 1985.

Podolske, J. R., M. Loewenstein, S. E. Strahan, and K. R. Chan, Stratospheric nitrous oxide distribution in the southern hemisphere, *J. Geophys. Res.*, in press, 1989.

Proffitt, M. H., et al., A chemical definition of the boundary of the Antarctic ozone hole, *J. Geophys. Res.*, this issue.

Schoeberl, M. R., et al., Reconstruction of the constituent distribution and trends in the Antarctic polar vortex from ER-2 flight observations, *J. Geophys. Res.*, in press, 1989.

Shine, K. P., On the modeled thermal response of the antarctic stratosphere to a depletion of ozone, *Geophys Res. Lett.*, *13*, 1331–1334, 1986.

Starr, W. L., and J. E. Vedder, Measurements of ozone in the Antarctic atmosphere during August and September 1987, *J. Geophys. Res.*, this issue.

Zhu, X., and J. R. Holton, Mean fields induced by local gravity-wave forcing in the middle atmosphere, *J. Atmos. Sci.*, *44*, 620–630, 1987.

K. R. Chan, M. Loewenstein, J. R. Podolske, and S. E. Strahan, NASA Ames Research Center, Moffett Field, CA 94035.

B. L. Gary, Jet Propulsion Laboratory, Pasadena, CA 91109.

D. L. Hartmann, Department of Atmospheric Sciences, AK-40, University of Washington, Seattle, WA 98195.

R. L. Martin, P. A. Newman, and M. R. Schoeberl, Laboratory for Atmospheres, NASA Goddard Space Flight Center, Greenbelt, MD 20771.

(Received June 16, 1988;
revised December 12, 1988;
accepted December 19, 1988.)